

Orbital Density Reconstruction for Molecules

M. Dauth, T. Körzdörfer, and S. Kümmel

Theoretical Physics IV, University of Bayreuth, D-95440 Bayreuth, Germany

J. Ziroff, M. Wiessner, A. Schöll, and F. Reinert

Experimental Physics 7 and Röntgen Research Center for Complex Material Systems (RCCM), University of Würzburg, D-97074 Würzburg, Germany

Karlsruhe Institute of Technology (KIT), Gemeinschaftslabor für Nanoanalytik, D-76021 Karlsruhe, Germany

M. Arita and K. Shimada

Hiroshima Synchrotron Radiation Center and Graduate School of Science, Hiroshima University, Hiroshima 739-8526, Japan
(Received 13 July 2011; published 4 November 2011)

The experimental imaging of electronic orbitals has allowed one to gain a fascinating picture of quantum effects. We here show that the energetically high-lying orbitals that are accessible to experimental visualization in general differ, depending on which approach is used to calculate the orbitals. Therefore, orbital imaging faces the fundamental question of which orbitals are the ones that are visualized. Combining angular-resolved photoemission experiments with first-principles calculations, we show that the orbitals from self-interaction-free Kohn-Sham density functional theory are the ones best suited for the orbital-based interpretation of photoemission.

DOI: 10.1103/PhysRevLett.107.193002

PACS numbers: 33.60.+q, 31.15.E-, 79.60.-i

Experiments that are interpreted as the visualization of molecular orbitals have become possible in rather different fields of science [1–3]. Angular-resolved photoemission spectroscopy (ARPES) has emerged as a particularly powerful tool [4–6], allowing one to visualize interface effects and substrate influences, thus gaining practical relevance by giving one access to properties that are fundamental to molecular electronics. However, the reconstruction of orbital densities is also fascinating from a fundamental point of view, as it allows one to visualize quantum mechanical properties that are considered elusive, revealing what is interpreted as a picture of the probability density for finding “an electron” in a molecule. However, for the very same reason, the results of “orbital measurements” may be debated: Nature does not know about one-electron orbitals, because electrons in a many-electron system are described by a correlated wave function and not by one-electron orbitals. Orbitals are a theoretical concept, introduced for noninteracting particles and used in interacting theories merely to build up a correlated wave function or to construct the density.

Typically, the photoemission intensity is written as [7]

$$I_f \propto \sum_i |\langle \Psi_f | \mathbf{A} \cdot \mathbf{p} | \Psi_i \rangle|^2 \delta(E_f - E_i - \hbar\omega) \quad (1)$$

for a transition from state $|\Psi_i\rangle$ to $|\Psi_f\rangle$ triggered by one photon of frequency ω in the semiclassical electromagnetic field \mathbf{A} . The final-state energy E_f is determined by the material’s work function and the kinetic energy of the measured electron. Writing the final state as an (antisymmetrized) product of a plane wave for the emitted electron

and the $N - 1$ electron state of the ionized system leads to a representation of the ionization process in terms of Dyson orbitals [8]. Even when the conditions under which the plane-wave approximation can be used [5] are fulfilled, it is not clear why the density of states on the right-hand side of Eq. (1) should be the one that one straightforwardly obtains from Hartree-Fock (HF) or density functional theory (DFT) calculations, and why ARPES should reflect the corresponding HF or DFT orbitals. In principle, the density of states should be the one of quasiparticles, e.g., as approximately obtained in a *GW* calculation [9]. The amazing observation is, though, that previous experiments could directly be related to the orbitals obtained from HF theory or semilocal density functional calculations. Here, we take this puzzle one step further and turn it into a serious question. We show that, for molecules that are of greater complexity than previously studied cases, different theories predict upper orbitals of different spatial character. What will orbital reconstruction techniques visualize in such cases? Combining first-principles calculations with ARPES experiments, we show that there is a systematic relation between the orbitals from self-interaction-free Kohn-Sham (KS) DFT and the measured intensities.

The orbital that typically is of greatest interest in orbital density reconstruction is the highest occupied molecular orbital (HOMO), and one of the so far largest molecules for which accurate orbital density visualization of the HOMO has been reported is pentacene [3,5,10]. In Ref. [5], ARPES data was explained based on generalized gradient approximation (GGA) orbitals, and our Fig. 1 confirms this approach: It hardly matters which theory is used to

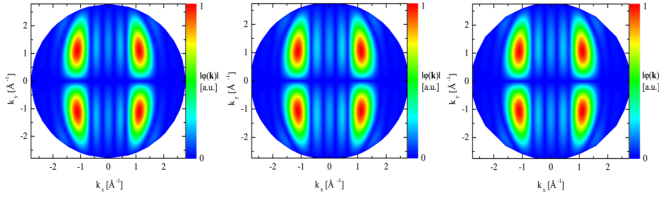


FIG. 1 (color online). Pentacene HOMO in momentum space. $|\varphi(\mathbf{k})|$ was evaluated on a hemisphere of radius $|\mathbf{k}| = 2.80 \text{ \AA}^{-1}$. Left: HF. Middle: PBE GGA [24]. Right: KS SIC [17].

calculate the HOMO. This is a consequence of pentacene’s simple electronic structure. The upper valence orbitals are delocalized on similar length scales; thus, the relative ordering of the orbitals and the momentum distributions are not sensitive to possible shortcomings of theoretical methods [11,12].

The situation changes for molecules of greater complexity. A prominent example in this respect is the 1,4,5,8-naphthalene-tetracarboxylic dianhydride (NTCDA) molecule. Neither HF nor GGAs lead to eigenvalues [13] that match the gas phase photoelectron spectrum [14]. Contracting [4] or stretching [15] theoretical spectra can improve spectral agreement. However, with the full momentum distribution available from ARPES, theory and experiment can be compared in much greater detail. Kera *et al.* [4] have shown in an important study that the ARPES for the NTCDA HOMO can be understood based on HF. However, GGAs yield different results, as shown below. So while for specific systems, HF or GGA-based DFT can yield a reliable description [4,5], there is the pressing question of whether there exists a theoretical approach which generally yields the correct orbital ordering and momentum distributions for molecules—in other words, which single-particle orbitals are the best approximation to Dyson orbitals. This question is at the heart of “molecular orbital reconstruction.”

To answer these questions, we investigate several single-particle approaches: HF and different density functionals, namely, the Perdew-Burke-Ernzerhof (PBE) GGA, the Becke three-parameter Lee-Yang-Parr (B3LYP) hybrid [16], and the KS self-interaction correction (SIC) functional. The KS SIC approach used here has been described in detail in Ref. [17]. Its essential feature is that a spatially local, multiplicative potential that is the same for all orbitals is constructed according to the generalized optimized effective potential equation (see [18] for technical details). In this way, the powerful arguments of KS theory can be brought to bear despite the functional’s orbital dependence.

There are pronounced differences between the NTCDA HOMOs obtained by different approaches. The top-left and top-middle panels of Fig. 2 show $|\varphi(\mathbf{k})| = |\int \varphi(\mathbf{r}) e^{-i\mathbf{k}\cdot\mathbf{r}} d^3r|$ of the NTCDA HOMO from the PBE and the KS SIC calculation, respectively, both evaluated at $|\mathbf{k}| = 2.75 \text{ \AA}^{-1}$ (see [18] for technical details). The

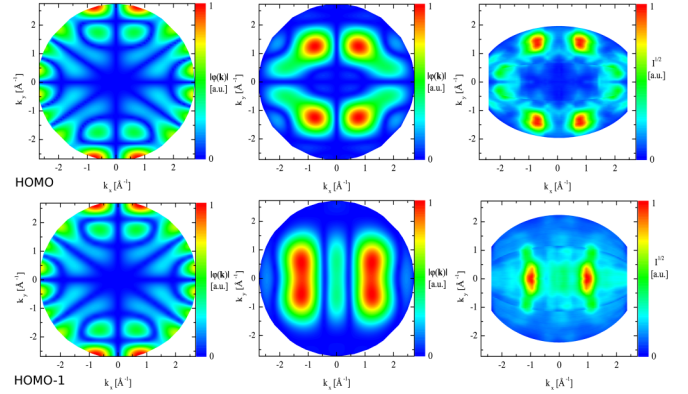


FIG. 2 (color online). Top: HOMO of NTCDA from PBE (left), KS SIC (middle), and square root of the ARPES intensity (right). Bottom: HOMO-1 from B3LYP (left), KS SIC (middle), and experiment (right).

observed marked differences have an important implication, because, as discussed in detail, e.g., in Ref. [5], $|\varphi(\mathbf{k})|$ can be related to the square root of the photoemission intensity. As the different calculations make rather different predictions for this quantity, NTCDA puts the orbital density interpretation to a serious test, allowing one to check which orbital, if any, will be seen in experiment.

The ARPES intensity distribution for the first emission peak is shown in the right plot of the top row of Fig. 2. The result is unambiguous: The experimental data reveal a close relation to the SIC orbital and none to the GGA orbital. The HOMO from HF and B3LYP (not shown) are similar to the SIC HOMO. The latter two approaches use integral-operator potentials, and the generalized Kohn-Sham equation resembles the Dyson equation [19,20]; thus, one may be tempted to believe that HF or hybrid functionals may approximate quasiparticle excitations better than any KS approach.

However, this is not the case, as seen by investigating the orbital below the HOMO, called HOMO-1 in the following. In the bottom row of Fig. 2, we compare $|\varphi(\mathbf{k})|$ for the HOMO-1 as found by B3LYP (left) and KS SIC (middle), each evaluated on a hemisphere of radius $|\mathbf{k}| = 2.73 \text{ \AA}^{-1}$, to the ARPES data (right). The SIC approach shows the experimentally observed features, whereas the B3LYP HOMO-1 does not resemble the experiment at all. The HF HOMO-1 (not shown) is similar to the HOMO-1 from KS SIC, but the characteristic “outward bending” seen experimentally for $k_x \approx \pm 1 \text{ \AA}^{-1}$, $k_y \geq 0.5 \text{ \AA}^{-1}$ is better reproduced by the SIC orbital. Furthermore, HF eigenvalues below HOMO-1 do not match the experiment at all, whereas the ones from self-interaction-free DFT are much more realistic, as shown in detail in Refs. [12,13]. Thus, we arrive at a decisive twofold insight. First, the orbital interpretation of photoemission can be used also for complex systems. Second, the self-interaction-free KS approach yields eigenvalues that reflect relative PES

peak positions and orbitals that correspond to ARPES intensities. It thus matches the “orbital density measurement” interpretation best.

This, of course, raises the question of whether one can understand why the orbitals from certain calculations cannot be related to the ARPES measurements. In KS DFT with its local multiplicative potential, the interpretabilities of orbitals and eigenvalues are closely tied to each other. Traditional DFT literature vigorously denied the KS eigenvalues any physical meaning. This, however, is not correct. Chong, Gritsenko, and Baerends [21] showed that KS eigenvalues can be very accurate approximations to the ionization potentials of upper valence electrons, and Duffy *et al.* [20] discussed in detail the relation between KS orbitals and Dyson orbitals. The decisive aspect for when an exchange-correlation functional will not yield physically interpretable eigenvalues and orbitals can be understood from Janak’s theorem [22], which states that relaxed ionization potentials can be obtained by integrating over the occupation number- (f -) dependent KS eigenvalues ε_i :

$$V_i = - \int_0^1 \varepsilon_i(f) df. \quad (2)$$

In a non-self-interaction-free KS calculation, the eigenvalues depend strongly and unphysically on the occupation numbers [11]. In KS approaches that eliminate self-interaction, the integrand in Eq. (2) does change much less over the integration range and can therefore be approximately taken out of the integral, and the eigenvalue at the upper integration limit approximately reflects the ionization potential. In other words, Kohn-Sham DFT can benefit from a cancellation of relaxation effects and “non-Koopmans” corrections. Earlier work gave semianalytical arguments for a near cancellation in atoms [11]. Our results show that in KS SIC the cancellation is excellent even for complex systems. Furthermore, any approach that is self-interaction-free and uses a multiplicative (KS) potential should yield physical orbitals and eigenvalues, and indeed we found that x -only optimized effective potential orbitals are qualitatively similar to the ones from KS SIC.

HF theory neglects correlation and does not employ a local multiplicative potential as KS theory does. Its eigenvalues correspond to an unrelaxed x -only approximation. They are thus less amenable to physical interpretation. The case of hybrid functionals is yet more involved. B3LYP combines $\approx 20\%$ of HF with a GGA, and thus the potential is neither self-interaction-free nor purely multiplicative—nevertheless, it yields eigenvalues that qualitatively often match photoemission peak positions [13,15], in particular, for NTCDA. However, the ARPES experiment presented here for the NTCDA HOMO-1 shows that the B3LYP orbital whose eigenvalue is at the right energy does not yield the experimentally observed momentum distribution; i.e., the energy agreement in this case is fortuitous.

As discussed in Refs. [4,5], scattering effects may influence the ARPES signal. Yet, for the present systems, their influence is much smaller [5] than the pronounced differences that are due to different molecular orbitals.

However, we can take the concept of measuring orbital densities to the edge by investigating a particularly challenging system. 3,4,9,10-perylene-tetracarboxylic acid dianhydride (PTCDA), another model organic semiconductor [6], is a complicated case, because different theoretical approaches agree on the structure of the HOMO, but the predictions for the lower lying orbitals differ largely, and there is not one distinct HOMO-1 but several energetically close-lying orbitals. We again focus on the PBE GGA and on KS SIC as the paradigm examples for a semilocal and self-interaction-free functional, respectively.

The PBE GGA finds two degenerate orbitals (HOMO-1 and HOMO-2) about 0.82 eV below the HOMO. The next orbital (HOMO-3) is energetically well separated from this degenerate pair, being lower by another 0.51 eV. The upper right plot in Fig. 3(a) shows the normalized sum of the absolute values of the Fourier transforms of the two degenerate GGA orbitals, evaluated at $|\mathbf{k}| = 1.92 \text{ \AA}^{-1}$. Based on the GGA calculation, one would thus expect one experimental peak about 0.82 eV below the HOMO peak that should be associated with a distinct ARPES intensity distribution.

The prediction from the KS SIC calculation is very different. SIC finds four orbitals in close energetic vicinity of each other. HOMO-1 lies 1.2 eV below the HOMO and is separated from HOMO-2 by just 0.19 eV. HOMO-2 itself is quasidegenerate (0.08 eV difference) with HOMO-3 and HOMO-4, the latter being strictly degenerate with each other. The lower left plot in Fig. 3(a) shows the absolute value of the Fourier transform of the SIC HOMO-1, the lower right the one of HOMO-2, and the upper left the normalized sum of the absolute values of the Fourier transforms of the two degenerate SIC orbitals HOMO-3 and HOMO-4. We used $|\mathbf{k}| = 1.92 \text{ \AA}^{-1}$ in each case. Thus, based on the SIC calculation, one expects that the ARPES intensity below the HOMO peak should have different contributions appearing in a rather small energy interval with distinctly different spatial patterns.

Turning to the ARPES experiment, one notes that, in contrast to the photoemission signals at the binding energies $E_B = 1.9 \text{ eV}$ and $E_B = 0.7 \text{ eV}$, which are directly assigned to the HOMO and the former lowest unoccupied molecular orbital, respectively, the signal between $E_B = 3.0 \text{ eV}$ and $E_B = 3.6 \text{ eV}$ (close to the onset of Ag 4d emission at $E_B \approx 4 \text{ eV}$) shows great complexity. A principal component analysis (see [18]) showed that at least four contributions need to be considered. We located these at binding energies of 3.1, 3.2, 3.3, and 3.5 eV. The corresponding data are shown in Fig. 3(b).

For the GGA calculation, neither the energetic position of the HOMO-1 nor the intensity pattern match the

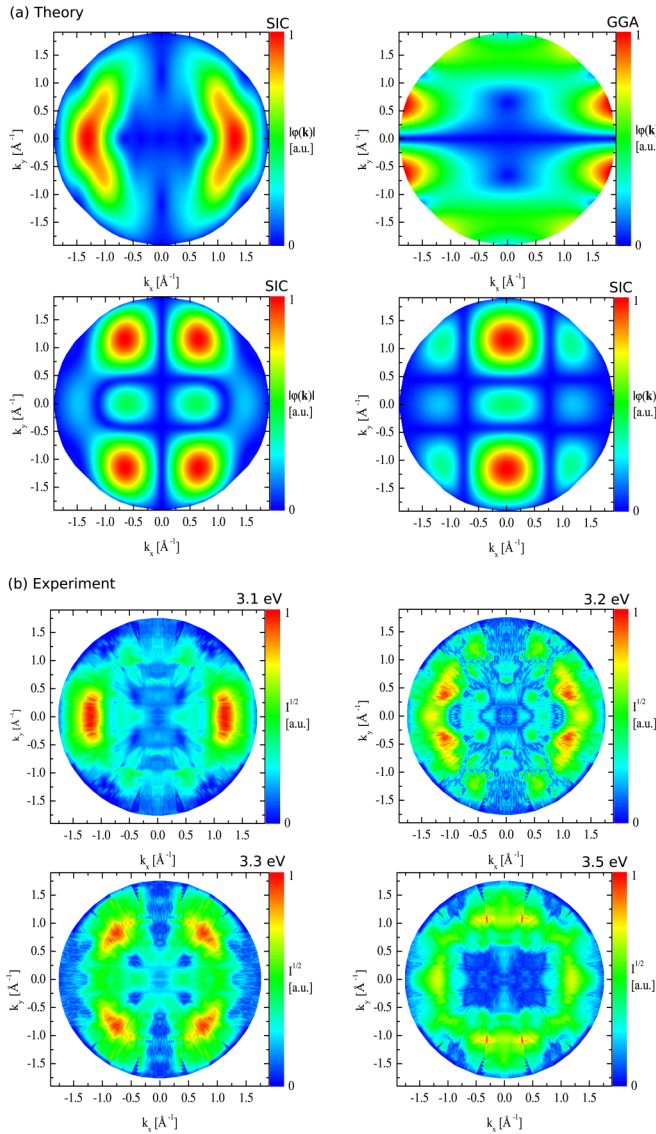


FIG. 3 (color online). (a) Absolute value of the Fourier transforms of PTCDA orbitals: SIC HOMO-1 (bottom left), SIC HOMO-2 (bottom right), normalized superposition of the degenerate SIC HOMO-3 and HOMO-4 (top left), and normalized superposition of the degenerate GGA HOMO-1 and HOMO-2 (top right). (b) Square root of the ARPES intensity at the four indicated binding energies.

experiment. The comparison of the experiment to the SIC calculation, on the other hand, is much clearer. The energetic separation between the HOMO and the next lower peak matches, and the experiment also very clearly confirms several different contributions. The intense signal at $E_B = 3.1$ eV is similar to the contribution one expects from the strictly degenerate SIC orbitals as seen in the upper left plot in Fig. 3(a). The measured intensity at $E_B = 3.3$ eV clearly reflects the lower left pattern in Fig. 3(a). Furthermore, the ARPES signal at $E_B = 3.5$ eV shows intensity at $k_x \approx 0$, $k_y = \pm 1 \text{ \AA}^{-1}$, which may stem from the orbital shown in the lower right plot in Fig. 3(a).

A finding that is puzzling at first sight is that the orbital ordering in the SIC calculation does not match the energetic ordering in which the corresponding ARPES intensities appear in the experiment, and we cannot determine unambiguously whether the experimental pattern at $E_B = 3.2$ eV should be reflected by a separate orbital. However, these discrepancies have a deeper reason, as can be seen from a comparison with a *GW* calculation for PTCDA [9]: *GW* predicts the same HOMO-1 pattern as KS SIC. This confirms that effects beyond the molecular orbital level must play a role.

At second sight, these discrepancies hardly come as a surprise given the complex situation that we investigate here. First, the Ag *d*-electron bands become increasingly important with increasing binding energy. Second, with the energetic differences between the SIC (or *GW*) orbitals being as small as found here, one cannot rule out that substrate influences or structural deformations such as bending [23] may change the ordering of the orbitals or may split degeneracies, and interactions between the various orbitals may be non-negligible. Yet, it is important to note that it can already be inferred from the calculation that the limits of the simple orbital interpretation are reached, as it results in a set of energetically close but spatially different orbitals.

In summary, we showed that for complex molecular systems different theories predict different upper orbitals, forcing us to face the question which of these orbitals, if any, can be related to experiments that are interpreted as measuring orbital densities. ARPES data unambiguously reveals a close correspondence to the orbitals from self-interaction-free KS theory, and we gave arguments for why this is the case. The combination of self-interaction-free density functional theory and angular-resolved photoemission reveals itself as a powerful tool for gaining insight into electronic properties.

S. K. acknowledges support by DFG GRK 1640 and GIF, T. K. by the AvH Foundation, F. R. and A. S. by DFG GRK 1221, FOR 1162, and the BMBF (Contracts No. 05K10WW2 and No. 03SF0356B), and F. R. and J. Z. from JSPS fellowships.

- [1] J. Itatani *et al.*, *Nature (London)* **432**, 867 (2004).
- [2] B. K. McFarland *et al.*, *Science* **322**, 1232 (2008).
- [3] J. Repp *et al.*, *Phys. Rev. Lett.* **94**, 026803 (2005).
- [4] S. Kera *et al.*, *Chem. Phys.* **325**, 113 (2006).
- [5] P. Puschnig *et al.*, *Science* **326**, 702 (2009).
- [6] J. Ziroff *et al.*, *Phys. Rev. Lett.* **104**, 233004 (2010).
- [7] S. Hüfner, *Photoelectron Spectroscopy* (Springer, Berlin, 2003), pp. 10–19.
- [8] M. Walter and H. Häkkinen, *New J. Phys.* **10**, 043018 (2008).
- [9] N. Dori *et al.*, *Phys. Rev. B* **73**, 195208 (2006).
- [10] J. Repp *et al.*, *Science* **312**, 1196 (2006).

- [11] J.P. Perdew and A. Zunger, *Phys. Rev. B* **23**, 5048 (1981).
- [12] T. Körzdörfer *et al.*, *Phys. Rev. B* **79**, 201205(R) (2009).
- [13] T. Körzdörfer, S. Kümmel, N. Marom, and L. Kronik, *Phys. Rev. B* **82**, 155206 (2010); **82**, 129903(E) (2010).
- [14] J. Sauther *et al.*, *J. Chem. Phys.* **131**, 034711 (2009).
- [15] N. Marom and L. Kronik, *Appl. Phys. A* **95**, 159 (2008).
- [16] P.J. Stephens *et al.*, *J. Phys. Chem.* **98**, 11 623 (1994).
- [17] T. Körzdörfer, M. Mundt, and S. Kümmel, *J. Chem. Phys.* **129**, 014110 (2008).
- [18] See Supplemental Material at <http://link.aps.org/supplemental/10.1103/PhysRevLett.107.193002> for details of our evaluation.
- [19] A. Seidl *et al.*, *Phys. Rev. B* **53**, 3764 (1996).
- [20] P. Duffy *et al.*, *Phys. Rev. A* **50**, 4707 (1994).
- [21] D.P. Chong, O. V. Gritsenko, and E. J. Baerends, *J. Chem. Phys.* **116**, 1760 (2002).
- [22] J.F. Janak, *Phys. Rev. B* **18**, 7165 (1978).
- [23] A. Hauschild *et al.*, *Phys. Rev. B* **81**, 125432 (2010).
- [24] J. P. Perdew, K. Burke, and M. Ernzerhof, *Phys. Rev. Lett.* **77**, 3865 (1996).